IOPscience iopscience.iop.org

Home Search Collections Journals About Contact us My IOPscience

Understanding doping at the nanoscale: the case of codoped Si and Ge nanowires

This content has been downloaded from IOPscience. Please scroll down to see the full text.

2014 J. Phys. D: Appl. Phys. 47 394013

(http://iopscience.iop.org/0022-3727/47/39/394013)

View the table of contents for this issue, or go to the journal homepage for more

Download details:

IP Address: 155.185.13.40
This content was downloaded on 12/09/2014 at 09:23

Please note that terms and conditions apply.

IOP Publishing Journal of Physics D: Applied Physics
J. Phys. D: Appl. Phys. 47 (2014) 394013 (10pp) doi:10.1088/0022-3727/47/39/394013

Understanding doping at the nanoscale: the case of codoped Si and Ge nanowires

Michele Amato[1], **Riccardo Rurali**[2], **Maurizia Palummo**[3] and **Stefano Ossicini**[4,5]

[1] Institut d'Electronique Fondamentale, UMR8622, CNRS, Université Paris Sud, 91405 Orsay, France
[2] Institut de Ciència de Materials de Barcelona (ICMAB-CSIC), Campus de Bellaterra, 08193 Bellaterra, Barcelona, Spain
[3] Dipartimento di Fisica, CNISM, ETSF Università di Roma 'Tor Vergata', Via della Ricerca Scientifica 1, 00133 Roma, Italy
[4] 'Centro S^3', CNR-Istituto di Nanoscienze, Via Campi 213/A, 41125 Modena, Italy and Dipartimento di Scienze e Metodi dell'Ingegneria, Università di Modena e Reggio Emilia, Via Amendola 2 Pad. Morselli, I-42100 Reggio Emilia, Italy
[5] Centro Interdepartmental En&Tech, Università di Modena e Reggio Emilia, Via Amendola 2 Pad. Morselli, I-42100 Reggio Emilia, Italy

E-mail: michele.amato@u-psud.fr

Received 17 March 2014, revised 4 June 2014
Accepted for publication 9 June 2014
Published 11 September 2014

Abstract

Results of first-principles DFT calculations of the structural and electronic properties of B–P codoped Si and Ge NWs are presented and discussed. We find that, according to experiments, for both Si and Ge NWs, impurities tend to get closer together and to occupy edge positions, as a result of minor structural relaxation and hence lower formation energy. The study of the electronic structure shows that the simultaneous addition of B and P only slightly modifies the energy band gap value with respect to the pure wire, and is strongly dependent on the particular codoping configuration considered.

Keywords: nanowires, doping, DFT, co-doping

(Some figures may appear in colour only in the online journal)

1. Introduction

Understanding of the doping mechanism at the nanoscale represents one of the main topics for the design and development of nanowire-based devices. Recent experimental and theoretical studies [1–9] on Si and Ge nanowires (NWs) have made concrete and real the possibility of using these one-dimensional nanostructures as corner-stones for the next generation electronics. Many applications using them as field-effect transistor (FET) [10, 11], p–n diode [12, 13], photovoltaic [14] and thermoelectric [15] devices have been demonstrated, and the scientific interest in this topic has been rapidly increasing in the last decade [16]. As for microelectronic technology, in all the above mentioned NW applications the possibility of modifying electronic properties of the material by introducing impurities is of paramount importance and its full understanding requires a microscopic picture of basic mechanisms. Many experimental and theoretical studies have addressed this topic [17–21], focusing mainly on B and P single doping of Si and Ge NWs. Experimentally, it has been clearly demonstrated that, with the current growth methods (such as vapour–liquid–solid growth [5]), it is possible to incorporate III and IV group impurities into the wire and to obtain both n-type and p-type wires [22–24]. On the other hand, theoretical investigations have shown that B and P impurities give rise to energetic levels deep in the band gap, and that they prefer to segregate towards the surface of the wire in order to minimize mechanical stress and distortions [17, 18, 25].

Very recently, the simultaneous addition of B and P impurities, i.e. codoping, has also been demonstrated to be a fundamental tool for modifying electronic and optical features of NWs [20]. As already shown for Si nanocrystals (NCs) [26–30], being able to control the band gap through double addition of impurities allows us to tune properties such as

 © 2014 IOP Publishing Ltd Printed in the UK

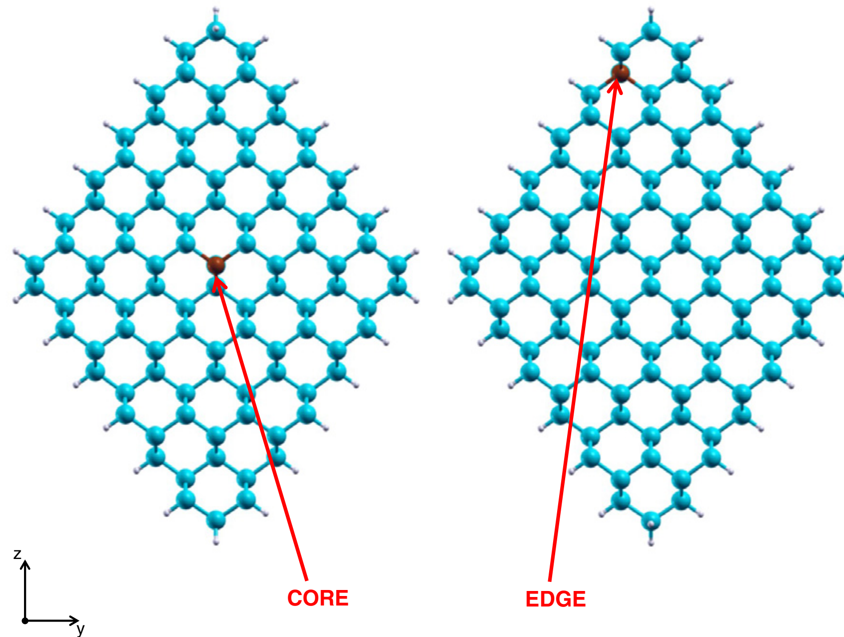

Figure 1. Top view of pure wires with a single impurity occupying a core site (left panel) and an edge site (right panel). Blue spheres can represent Si or Ge atoms, magenta spheres impurity atoms, while the small white spheres are H atoms used to saturate the dangling bonds.

absorption and photoluminescence. Nevertheless, unlike the case of B and P single doped systems, very few theoretical studies [18, 21] have addressed the analysis of B–P codoped Si NWs, and moreover they have been mainly focused on very thin NWs (with diameters up to 1.6 nm) and with doping concentrations too high to be compared with experiments. Furthermore, up to now, no works have been dedicated to the study of codoped Ge NWs. Other works addressed doping with more impurities of the same chemical species to study the stability of dopant pairs [31–33].

The purpose of this article is to fill this gap, by studying the formation energies (FEs) and the electronic properties of B–P codoped Si and Ge NWs by means of *ab initio* calculations. In particular, we show that (i) in B–P codoped Si and Ge wires, impurities tend to get closer together and to occupy edge positions, (ii) the simultaneous addition of B and P only slightly modifies the energy band gap value with respect to the pure wire, and (iii) localization of electronic states and the energy position of impurity levels is strictly related to the particular codoping configuration considered. The article is organized as follows. Section 2 contains the description of the method used for our calculations and the details of the geometry of our wires. Section 3 presents calculations of impurity FEs for both Si and Ge NWs, while section 4 is dedicated to the analysis of band structure and electronic properties. In section 5 we draw some conclusions and make final remarks.

2. Methods

We have studied [1 1 0] oriented B–P codoped Si and Ge NWs with a diameter of 2.4 nm. The top view of the wire's geometry is presented in figure 1. The atomic structure has been derived from the bulk diamond geometry by following the procedure adopted in [34–37]. At these small dimensions, surface reconstruction effects can strongly affect the electronic structure of the material. Indeed it has been demonstrated that reorganization of surface atoms can induce a metallic and semi-metallic behaviour into the wire [38–40]. However, since we are only interested in the description of semiconducting NWs, all the surface atoms of our model have been hydrogenated and no surface reconstruction has been considered. In this way, surface dangling bonds are completely saturated with hydrogen atoms and all the intra-gap states are eliminated. Moreover, the use of such a model, as is common in this type of investigation on doped nanostructures (see [16] and references therein), permits us to clearly identify the nature of defect states in the semiconductor band gap. B and P have been considered as substitutional impurities in both core and edge lattice sites, as shown in figure 1. Further details of the geometry of the wires can be found in [34–37]. It is worth noting that, in order to eliminate the spurious interaction between the periodic images of impurities and to obtain converged results for the FE [41], we have used a supercell that is six times the unit cell along the wire axis (more than 700 hundred atoms) and vacuum buffer of nearly 10 Å (see figure 2). This kind of supercell provides a dopant concentration comparable with the high doping regime of several experimental studies on NWs [42, 43]. For both Si and Ge NWs, we have analyzed four different configurations: (i) the n-type edge–p-type core configuration, in which P occupies an edge site, while B is located in the core of the wire (see figure 2(*a*)), (ii) the p-type edge–n-type core configuration, in which P is in the core and B at the edge of the wire (equivalent to figure 2(*a*) but with atoms switched), (iii) the n-type edge–p-type edge configuration, in which both P and B occupy an edge site (see figure 2(*b*)), (iv) the n-type core–p-type core configuration, in which both P and B occupy a core site (see figure 2(*c*)). The relative distance between impurities (red vector of figure 2) varies

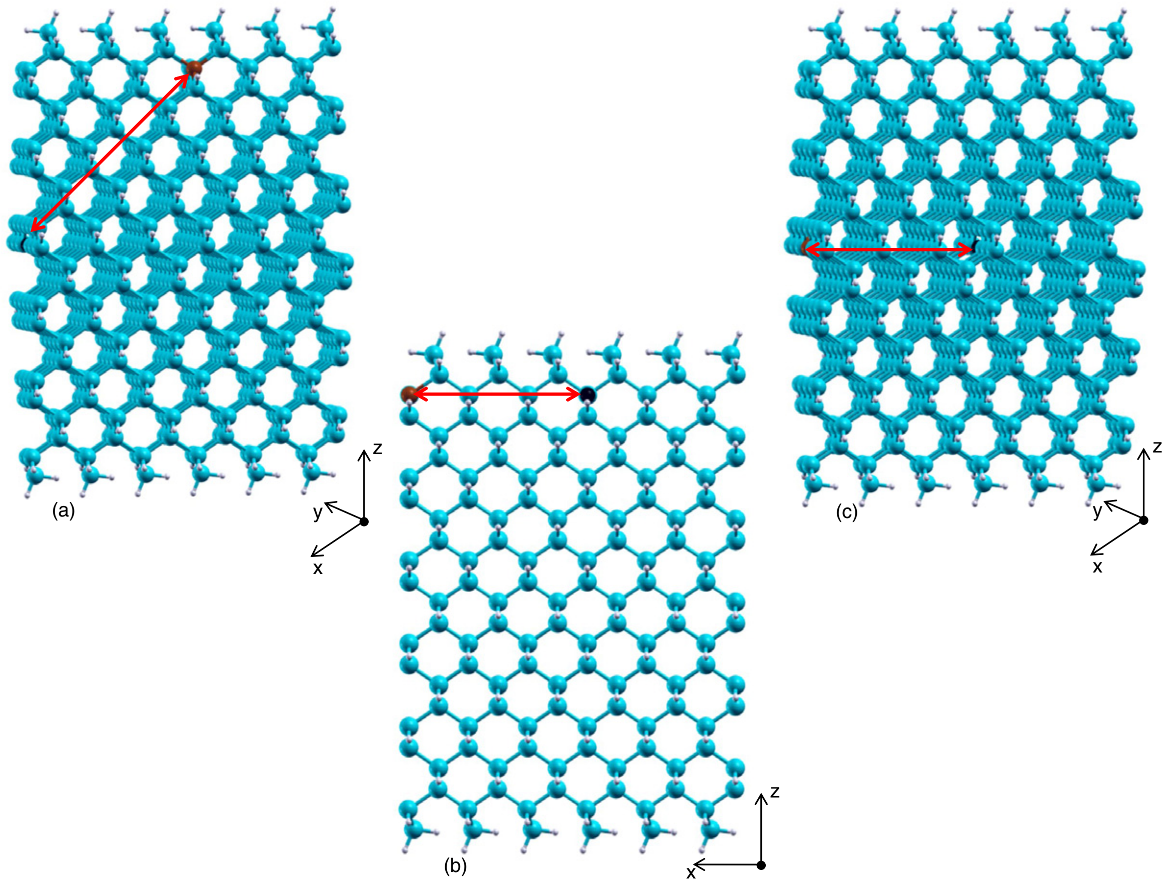

Figure 2. Side view of codoped Si and Ge NWs for three types of codoping configuration: core–edge (*a*), edge–edge (*b*) and core–core (*c*) configurations. Blue spheres can represent Si or Ge atoms, magenta and black P and B atoms respectively, while the small white spheres are H atoms used to saturate the dangling bonds.

Table 1. Calculated relative distance between impurities (red vector of figure 2) (in Å) for Si NWs (first row) and Ge NWs (second row) for all the codoping configurations considered.

	B core–P edge	P core–B edge	B core–P core	B edge–P edge
Si NWs	16.84	16.84	11.49	11.48
Ge NWs	17.53	17.53	12.06	12.06

when different impurity substitutional sites are considered: particular configurations with a dopant in the core and the other one in the shell present a longer relative distance with respect to configurations with dopants in the same region of the wire (i.e. core–core or edge–edge). Numerical values for the red vector in each relaxed geometry are reported in table 1.

All the calculations have been performed in the framework of density functional theory (DFT) as implemented in the SIESTA code [44]. The local density approximation (LDA) has been adopted for the exchange-correlation functional. Norm conserving pseudo-potentials for the core electronic states have been used, and the one-electron wave function of valence states has been expanded with a double-ζ basis set plus polarization functions. As all the considered codoped wires have an even number of electrons due to the compensation of the donor (P atom) and acceptor (B atom), no spin polarization effects have been included in the calculations. All the geometries have been fully relaxed until all the forces were lower than 0.04 eV Å^{-1} (this criterion, which represents a good compromise between accuracy and computational effort, has already been demonstrated to be successful in the description of the electronic properties of Si, Ge and SiGe NWs; see, for example, [36]). Due to the large dimension of the supercell in the periodic direction, the Brillouin zone has been sampled with the Γ point only. No sampling of the Brillouin zone along the transversal directions is required, because the system is not periodic in that direction. However, upon relaxation, the electronic structure has been evaluated with a finer grid of $(1 \times 1 \times 16)$. Forces on the atoms have still been found to be lower than 0.04 eV Å^{-1}, confirming the results of Γ point relaxations. We are aware that refined excited-state GW calculations [45] should be performed to have a correct estimation of the electronic impurity levels; nevertheless, the huge size of our simulation cell prevents the use of these approaches. In any case, the trend indicated by our study regarding the electronic properties of codoped Si and Ge NWs is certainly valid at least at the qualitative level.

3. Formation energies

As a first step, we have evaluated the FE, i.e. the energetic cost of adding an impurity to or removing it from a pure wire, for B

Table 2. Calculated FE (in eV) for Si NWs (first row) and Ge NWs (second row) for all the codoping configurations considered.

	B core–P edge	P core–B edge	B core–P core	B edge–P edge
Si NWs	−10.65	−10.84	−11.77	−11.92
Ge NWs	−10.24	−10.47	−11.82	−12.14

and P impurities in both Si and Ge NWs. Our FE calculations are performed using the Zhang and Northrup formalism [46] and, in particular, its reformulation especially developed for NWs by Rurali and Cartoixà [47]. In table 2 we summarize our main results.

Looking at table 2, one can draw several main conclusions valid for both Si and Ge NWs. (i) B and P impurities have a tendency to sit close together. Indeed the configurations with smaller relative distance between them (P core–B core and P edge–B edge) are energetically preferred (i.e., they present the lowest FE, as shown in table 2. (ii) Among these two lowest FE configurations, the one in which impurities occupy edge sites (P edge–B edge) is preferred, as a consequence of the greater freedom of mechanical relaxation, as explained in depth in [18] and as confirmed by experiments. (iii) Among the two highest FE configurations (B core–P edge and P core–B edge), the most stable is the one with a P atom occupying a core site and a B atom at the edge of the wire. The origin of this physical behaviour can be explained using segregation energy arguments discussed in [17, 18]. In their works the authors evaluated for B and P single doped Si and Ge NWs the segregation energy of an impurity, E_s, defined as the total energy difference between an NW doped in the core and one doped at its edge. They found that, for both Si and Ge NWs, the E_s of a P impurity is always smaller than the one for B (this means that the energetic gain of moving a B atom from the core to the edge of the wire is higher with respect to the gain for a P atom, hence there will not be much energetic difference for P atoms to segregate towards the surface or to occupy core sites). For this reason, in our case, among the two highest FE configurations (B core–P edge and P core–B edge), the most stable one presents a P atom in the core.

Hence our results can be summarized as follows: (i) in B–P codoped Si and Ge wires, impurities tend to get closer together and to occupy edge positions and (ii) P atoms will have a preference to sit in inner subsurface sites. This very interesting behaviour can be used to confirm the structural model proposed by Sugimoto *et al* [49] in the case of colloidal codoped Si NCs. In their work, they clearly explained that codoping of NCs is an essential condition to have high dispersibility in solution, and that a possible origin of this mechanism is the presence of P–B pairs on the subsurface, that, inducing a negative surface potential, can inhibit agglomeration. The model they propose, presenting B atoms on the surface and P atoms in inner positions, has been theoretically successfully discussed in the case of Si NCs [48], and is perfectly supported by our results and by the energetic considerations mentioned above.

Table 3. DFT-LDA electronic band gaps (in eV) for pure NWs (first column), codoped P core–B edge configuration (second column) and B core–P edge configuration (third column) for both Si (first row) and Ge NWs (second row).

	pure	B core–P edge	P core–B edge	B core–P core	B edge–P edge
Si NWs	0.97	0.81	0.80	0.91	0.96
Ge NWs	0.78	0.66	0.67	0.70	0.74

4. Electronic properties

In this section we present results regarding calculations of electronic structure for codoped Si and Ge NWs. As already demonstrated in the case of codoped Si NCs [27], the main effect of codoping should be to introduce impurity energetic levels into the gap, modifying the energy band gap value and electronic state localizations. However, this doping mechanism slightly changes in the case of Si and Ge NWs. As a first step, in table 3, we have reported the values of the DFT electronic band gap for all the codoping configurations considered as well as for the pure NWs. Looking at the numerical values one can draw two main conclusions: (i) the impurity states slightly modify the band gap of the pure wire, in contrast with what was observed in the case of Si NCs (in which the variation of the band gap with respect to the pure case was of the order of 0.7 eV), (ii) the magnitude of this reduction depends on the particular geometry considered, as well as the relative distance between impurities. As regards the first point, by looking at table 3, we can say that, for both Si and Ge NWs, the B core–P edge and P core–B edge configurations present the greatest diminution of the band gap (however, this value is always less than 0.2 eV for both Si and Ge NWs and really small if compared to the reduction observed for Si NCs). The core–core configuration has the smallest gap variation with respect to the pure wires, but the reduction is less than 0.1 eV. Finally, the edge–edge configuration represents the most interesting case, since it has the same band gap as the pure NWs. To rationalize these results, we note that in the case of codoped Si NCs the following have been proved [28]: (i) the diminution of the band gap depends on the dimension of the NCs; i.e., the impurity related levels are less and less deep in the undoped semiconductor band gap for larger NCs. Thus the reduction of the band gap is an inverse function of the ratio between the number of impurities and the number of Si or Ge atoms in the nanostructures; this ratio being much smaller in the case of NWs with respect to NCs, the reduction of the band gap is smaller for NWs than for NCs. (ii) The reduction also depends on the distance between impurities. As a consequence of enhanced Coulomb interaction smaller distances originate larger gaps, i.e. smaller reductions; this trend is here confirmed for NWs. In order to obtain some insight into this observation, in figures 3–8 we plot, for all the considered wires, the band structure and the wave function localizations of band edges.

The comparison of band structures of codoped wires with pure wires (not shown here) has indicated that the introduction of impurities does not change too much the dispersion of the states, which essentially preserves the same shape. On the other hand, the analysis of the wave function localizations

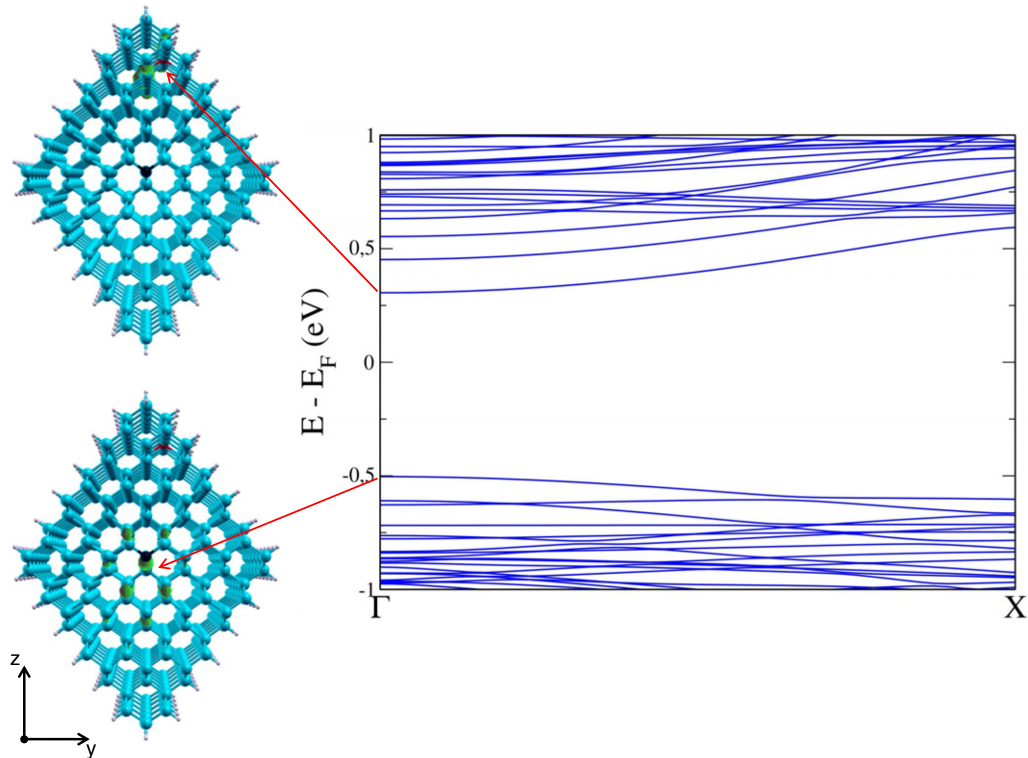

Figure 3. DFT electronic band structure for B core–P edge doped Si NWs (right panel). The spatial localization of the impurity state wave function (in green) is also shown (left panel). Blue spheres represent Si atoms, magenta and black P and B atoms respectively, while the small white spheres are H atoms used to saturate the dangling bonds.

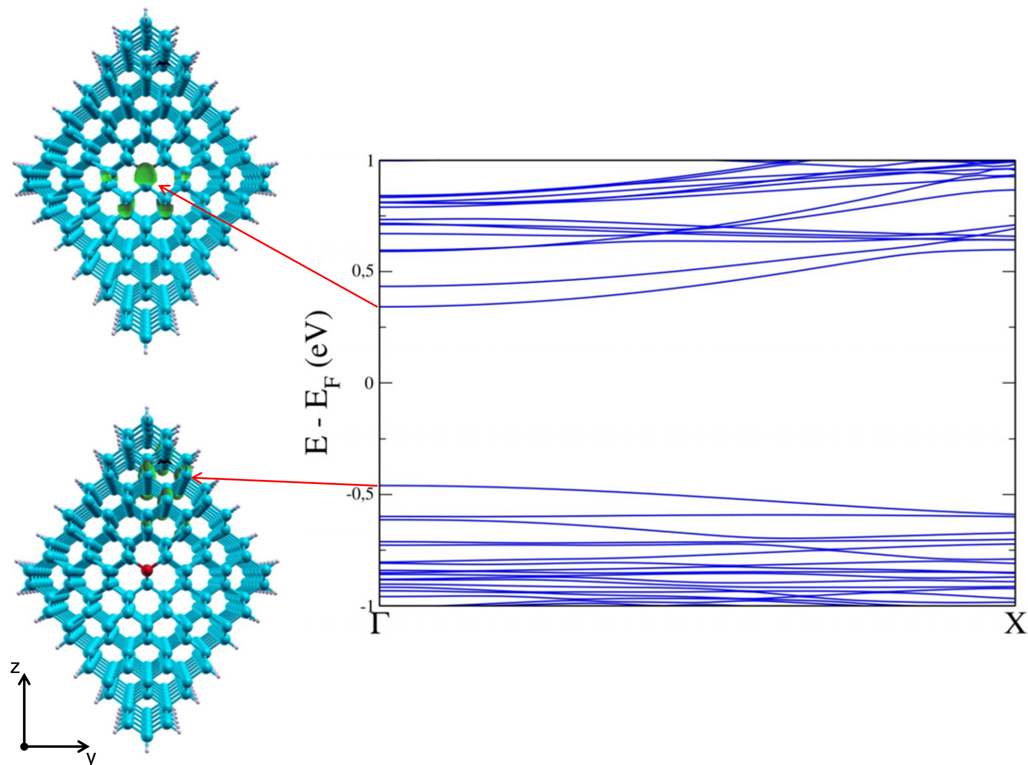

Figure 4. DFT electronic band structure for P core–B edge doped Si NWs (right panel). The spatial localization of the impurity state wave function (in green) is also shown (left panel). Blue spheres represent Si atoms, magenta and black P and B atoms respectively, while the small white spheres are H atoms used to saturate the dangling bonds.

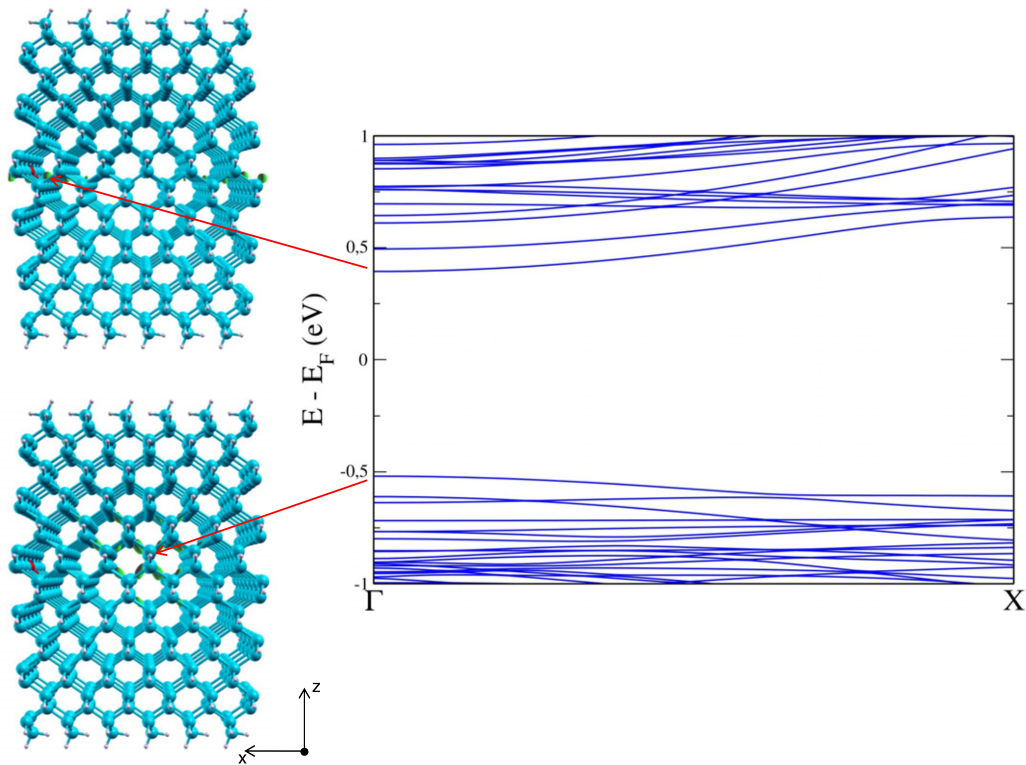

Figure 5. DFT electronic band structure for B core–P core doped Si NWs (right panel). The spatial localization of the impurity state wave function (in green) is also shown (left panel). Blue spheres represent Si atoms, magenta and black P and B atoms respectively, while the small white spheres are H atoms used to saturate the dangling bonds.

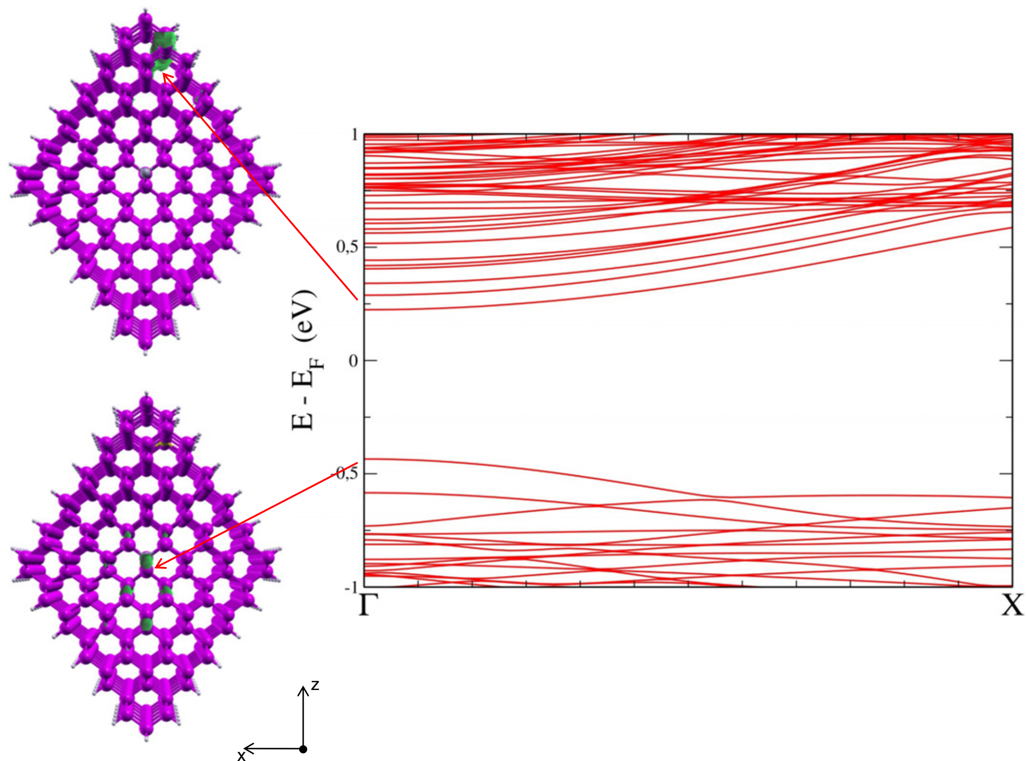

Figure 6. DFT electronic band structure for B core–P edge doped Ge NWs (right panel). The spatial localization of the impurity state wave function (in green) is also shown (left panel). Magenta spheres represent Ge atoms, yellow and brown P and B atoms respectively, while the small white spheres are H atoms used to saturate the dangling bonds.

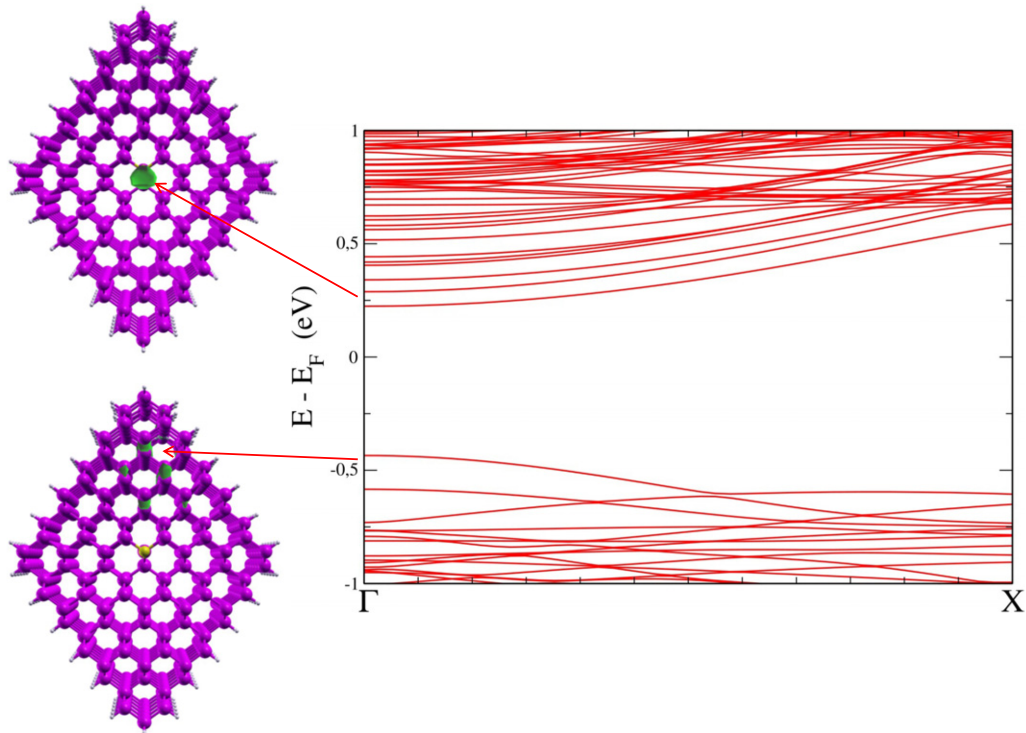

Figure 7. DFT electronic band structure for P core–B edge doped Ge NWs (right panel). The spatial localization of the impurity state wave function (in green) is also shown (left panel). Magenta spheres represent Ge atoms, yellow and brown P and B atoms respectively, while the small white spheres are H atoms used to saturate the dangling bonds.

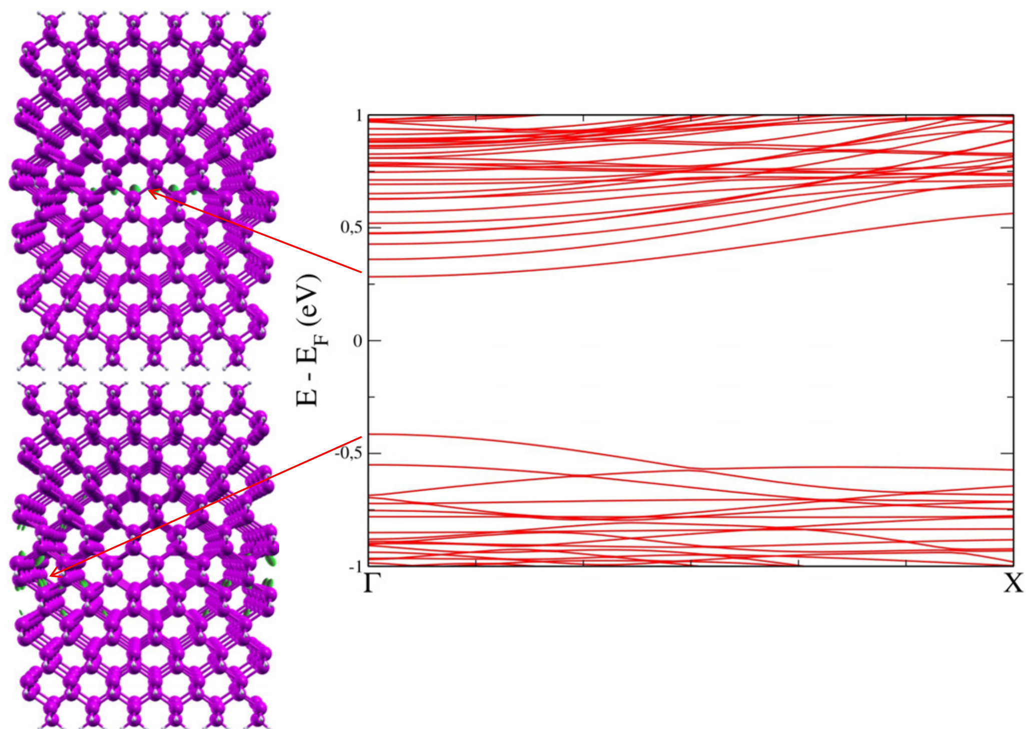

Figure 8. DFT electronic band structure for B core–P core doped Ge NWs (right panel). The spatial localization of the impurity state wave function (in green) is also shown (left panel). Magenta spheres represent Ge atoms, yellow and brown P and B atoms respectively, while the small white spheres are H atoms used to saturate the dangling bonds.

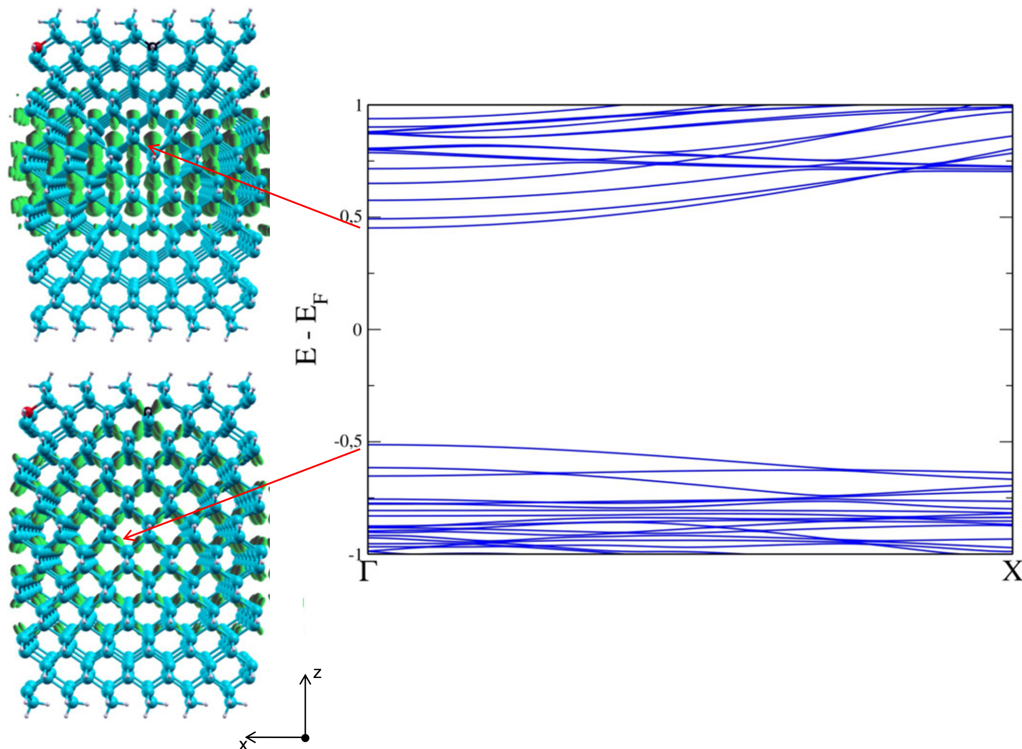

Figure 9. DFT electronic band structure for B edge–P edge doped Si NWs (right panel). The spatial localization of the impurity state wave function (in green) is also shown (left panel). Blue spheres represent Si atoms, magenta and black P and B atoms respectively, while the small white spheres are H atoms used to saturate the dangling bonds.

of band edges (see left panel of figures 3–8) for codoped wires show that the top of the valence band is located at the B impurity, while the bottom of the conduction band is located at P. This behaviour is responsible for the reduction of band gap we observe here, and has the same physical nature already demonstrated both theoretically and experimentally in the case of codoped Si NCs [26, 27]. Furthermore, our results are qualitatively in agreement with the theoretical calculations of [18] for thinner wires and with a supercell made by only four unit cells.

The only exception to this behaviour is represented by the edge–edge configuration, in which, for both Si and Ge NWs, the impurity states do not occupy both the band edges. In particular, for edge–edge Ge NWs (see figure 10) the valence band maximum is located on Ge while the conduction band minimum is located on the P atom, while for edge–edge Si NWs (see figure 9) the valence band maximum and conduction band minimum are both localized on Si and the impurity states are deep in the valence and conduction states. In our opinion, this is due to the different screening effects at work at the edge and in the interior of the NWs.

5. Conclusions

We have presented first-principles DFT calculations on the structural and electronic properties of B–P codoped Si and Ge NWs. For the first time in the study of codoped wires, diameters larger than 2 nm and high doping regime concentrations have been considered. Our results demonstrate that, for both Si and Ge NWs, impurities tend to get closer together and to occupy edge positions, resulting in lower FE. Moreover, the electronic property analysis shows that the codoping is responsible, in both Si and Ge NWs, for a minimal reduction of the band gap with respect to the pure wires. This finding can play a particular role in view of Si NWs solar cell devices: in fact, we have demonstrated that the codoping process, fundamental for the fabrication of radial and axial p–n junctions, does not affect the band gap value, preserving the quantum confinement regime and the associated optical absorption spectra. Finally we have shown that, for both Si and Ge NWs, the codoping configuration also has an influence on the electronic state localizations.

Acknowledgments

MA gratefully acknowledges the Transnational Access Programme of the HPC-EUROPA2 Project. SO acknowledges the European Community's Seventh Framework Programme (FP7/2007-2013) under grant agreement 245977, Ministero Affari Esteri, Direzione Generale per la Promozione e la Cooperazione Culturale. M.P. acknowledges the Ec e-I3 ETSF project (INFRA No 211956). The authors gratefully acknowledge the computer resources, technical expertise and assistance provided by the Red Española de Supercomputaciòn and the CINECA award under the ISCRA initiative (No HP10BQNB3U and No HP10B2DDQJ) for the availability of high performance computing resources and support. Funding under contract Nos FEDER-FIS2012-37549-C05-05 and CSD2007-00041 of the Ministerio de Economía y

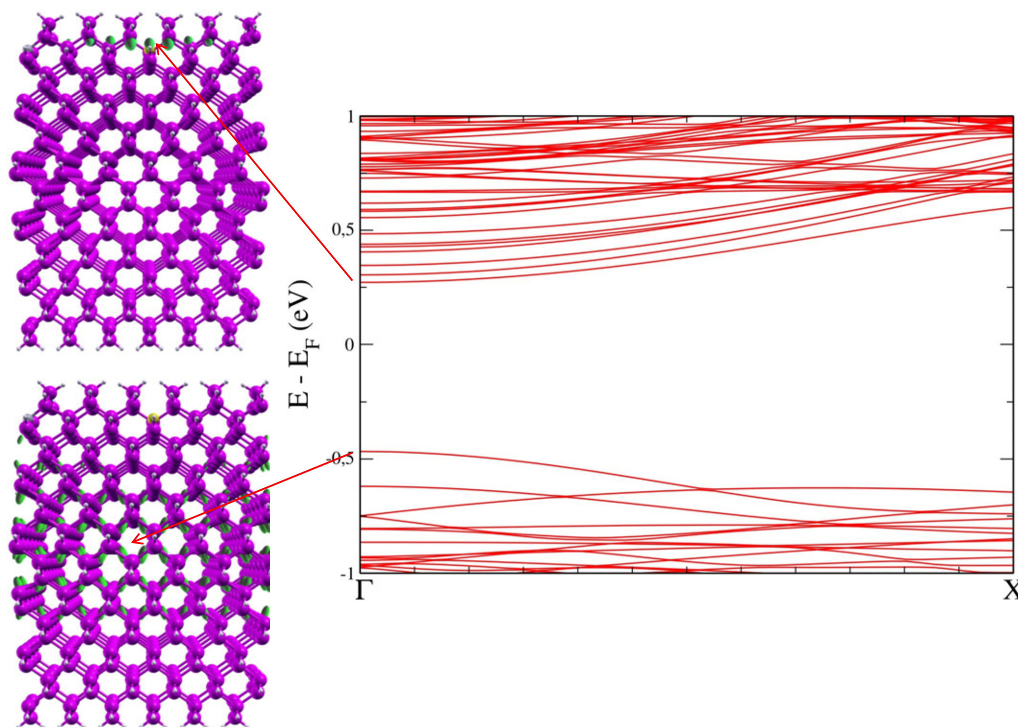

Figure 10. DFT electronic band structure for B edge–P edge doped Ge NWs (right panel). The spatial localization of the impurity state wave function (in green) is also shown (left panel). Magenta spheres represent Ge atoms, yellow and brown P and B atoms respectively, while the small white spheres are H atoms used to saturate the dangling bonds.

Competitividad (MINECO) and computational resources at the Centro de Supercomputación de Galicia (CESGA) are gratefully acknowledged.

References

[1] Yan H, Choe H S, Nam S W, Hu Y, Das S, Klemic J F, Ellenbogen J C and Lieber C M 2011 *Nature* **470** 240–4
[2] Hu Y, Xiang J, Liang G, Yan H and Lieber C M 2008 *Nano Lett.* **8** 925–30
[3] Cui Y, Zhong Z, Wang D, Wang W U and Lieber C M 2003 *Nano Lett.* **3** 149–52
[4] Hu Y, Churchill H O H, Reilly D J, Xiang J, Lieber C M and Marcus C M 2007 *Nature Nanotech.* **2** 622–5
[5] Cui Y and Lieber C M 2001 *Science* **291** 851–3
[6] Berkdemir C and Gülseren O 2009 *Phys. Rev.* B **80** 115334
[7] Peng X, Tang F and Logan P 2011 *J. Phys.: Condens. Matter* **23** 115502
[8] Hasan M, Huq M F and Mahmood Z H 2013 *SpringerPlus* **2** 151
[9] Amato M, Palummo M, Rurali R and Ossicini S 2014 *Chem. Rev.* **114** 1371–412
[10] Gao X P A, Zheng G and Lieber C M 2010 *Nano Lett.* **10** 547–52
[11] Huang Y, Duan X, Cui Y, Lauhon L J, Kim K H and Lieber C M 2001 *Science* **294** 1313–7
[12] Hayden O, Agarwal R and Lieber C M 2006 *Nature Mater.* **5** 352–6
[13] Fung W Y, Chen L and Lu W 2011 *Appl. Phys. Lett.* **99** 092108
[14] Kelzenberg M D, Boettcher S W, Petykiewicz J A, Turner-Evans D B, Putnam M C, Warren E L, Spurgeon J M, Briggs R M, Lewis N S and Atwater H A 2010 *Nature Mater.* **9** 239–44
[15] Hochbaum A I, Chen R, Diaz Delgado R, Liang W, Garnett E C, Najarian M, Majumdar A and Yang P 2008 *Nature* **451** 163–7
[16] Rurali R 2010 *Rev. Mod. Phys.* **82** 427–49
[17] Peelaers H, Partoens B and Peeters F M 2007 *Appl. Phys. Lett.* **90** 263103
[18] Peelaers H, Partoens B and Peeters F M 2006 *Nano Lett.* **6** 2781–4
[19] Fukata N, Chen J, Sekiguchi T, Matsushita S, Oshima T, Uchida N, Murakami K, Tsurui T and Ito S 2007 *Appl. Phys. Lett.* **90** 153117
[20] Fukata N, Mitome M, Bando Y, Seoka M, Matsushita S, Murakami K, Chen J and Sekiguchi T 2008 *Appl. Phys. Lett.* **93** 203106
[21] Palummo M, Iori F, Sole R D and Ossicini S 2009 *Superlatt. Microstruct.* **46** 234–9
[22] Pavlov S G, Eichholz R, Abrosimov N V, Redlich B and Hubers H W 2011 *Appl. Phys. Lett.* **98** 061102
[23] Nah J, Varahramyan K, Liu E S, Banerjee S K and Tutuc E 2008 *Appl. Phys. Lett.* **93** 203108
[24] Fukata N 2009 *Adv. Mater.* **21** 2829–32
[25] Leão C R, Fazzio A and da Silva A J R 2008 *Nano Lett.* **8** 1866–71
[26] Fujii M, Yamaguchi Y, Takase Y, Ninomiya K and Hayashi S 2004 *Appl. Phys. Lett.* **85** 1158–60
[27] Ossicini S, Degoli E, Iori F, Luppi E, Magri R, Cantele G, Trani F and Ninno D 2005 *Appl. Phys. Lett.* **87** 173120
[28] Iori F, Degoli E, Magri R, Marri I, Cantele G, Ninno D, Trani F, Pulci O and Ossicini S 2007 *Phys. Rev.* B **76** 085302
[29] Ramos L E, Degoli E, Cantele G, Ossicini S, Ninno D, Furthmüller J and Bechstedt F 2008 *Phys. Rev.* B **78** 235310
[30] Fujii M, Yamaguchi Y, Takase Y, Ninomiya K and Hayashi S 2005 *Appl. Phys. Lett.* **87** 211919
[31] Moon C-Y, Lee W-J and Chang K J 2008 *Nano Lett.* **8** 3086–91

[32] Park J-S, Ryu B and Change K J 2011 *J. Phys. Chem.* C **115** 10345–50
[33] Kim S, Park J-S and Chang K J 2012 *Nano Lett.* **12** 5068–73
[34] Amato M, Palummo M and Ossicini S 2009 *Phys. Rev.* B **80** 235333
[35] Amato M, Palummo M and Ossicini S 2009 *Phys. Rev.* B **79** 201302(R)
[36] Amato M, Ossicini S and Rurali R 2011 *Nano Lett.* **11** 594–8
[37] Amato M, Palummo M and Ossicini S 2010 *Phys. Status Solidi* b **247** 2096
[38] Rurali R and Lorente N 2005 *Phys. Rev. Lett.* **94** 026805
[39] Rurali R and Lorente N 2005 *Nanotechnology* **16** S250
[40] Rurali R, Poissier A and Lorente N 2006 *Phys. Rev.* B **74** 165324
[41] Rurali R, Palummo M and Cartoixà X 2010 *Phys. Rev.* B **81** 235304
[42] Nah J, Liu E S, Shahrjerdi D, Varahramyan K M, Banerjee S K and Tutuc E 2009 *Appl. Phys. Lett.* **94** 063117
[43] Wang Y, Lew K K, Ho T T, Pan L, Novak S W, Dickey E C, Redwing J M and Mayer T S 2005 *Nano Lett.* **5** 2139–43
[44] Soler J M, Artacho E, Gale J D, García A, Junquera J, Ordejón P and Sánchez-Portal D 2002 *J. Phys.: Condens. Matter* **14** 2745–79
[45] Niquet Y M, Genovese L, Delerue C and Deutsch T 2010 *Phys. Rev.* B **81** 161301
[46] Zhang S B and Northrup J E 1991 *Phys. Rev. Lett.* **67** 2339–42
[47] Rurali R and Cartoixà X 2009 *Nano Lett.* **9** 975–9
[48] Guerra R and Ossicini S 2014 *J. Am. Chem. Soc.* **136** 4404–9
[49] Sugimoto H, Fujii M, Imakita K, Hayashi S and Akamatsu K 2012 *J. Phys. Chem.* C **116** 17969–74